

Soft Matter

Accepted Manuscript



This is an *Accepted Manuscript*, which has been through the Royal Society of Chemistry peer review process and has been accepted for publication.

Accepted Manuscripts are published online shortly after acceptance, before technical editing, formatting and proof reading. Using this free service, authors can make their results available to the community, in citable form, before we publish the edited article. We will replace this *Accepted Manuscript* with the edited and formatted *Advance Article* as soon as it is available.

You can find more information about *Accepted Manuscripts* in the [Information for Authors](#).

Please note that technical editing may introduce minor changes to the text and/or graphics, which may alter content. The journal's standard [Terms & Conditions](#) and the [Ethical guidelines](#) still apply. In no event shall the Royal Society of Chemistry be held responsible for any errors or omissions in this *Accepted Manuscript* or any consequences arising from the use of any information it contains.

Morphological changes of amphiphilic molecular assemblies induced by chemical reaction

Koh M. Nakagawa and Hiroshi Noguchi*

Received Xth XXXXXXXXXXXX 20XX, Accepted Xth XXXXXXXXXXXX 20XX

First published on the web Xth XXXXXXXXXXXX 200X

DOI: 10.1039/b000000x

Shape transformations of amphiphilic molecular assemblies induced by chemical reaction are studied using coarse-grained molecular simulations. A binding reaction between hydrophilic and hydrophobic molecules is considered. It is found that the reaction induces transformation of an oil droplet to a tubular vesicle via bicelles and vesicles with discoidal arms. The discoidal arms close into vesicles, which are subsequently fused into the tubular vesicle. Under the chemical reaction, the bicelle-to-vesicle transition occurs at smaller sizes than in the absence of the hydrophobic molecules. It is revealed that the enhancement of this transition is due to embedded hydrophobic particles that reduce the membrane bending rigidity.

1 Introduction

Amphiphilic molecules in an aqueous solution spontaneously aggregate into various structures. Depending on the molecular structure, different self-assembled structures appear, *e.g.*, spherical and worm-like micelles, vesicles, bicontinuous structures, etc^{1–3}. In particular, the morphology of vesicles attracts the attention of many researchers, as this is the simplest model of a cell membrane. Bilayer vesicles exhibit various shapes, *e.g.*, discocyte (red-blood-cell shape), single and double stomatocytes, tubulation, pearl-necklace shapes, and so on^{4–8}. Thus, static vesicle shapes have been well explored. In living cells, however, membrane sizes are dynamically changed by the moments of the fusion and fission of small vesicles. The lipid composition of biomembranes varies depending on the organelle and cell type, and the asymmetric distribution of the lipids between inner and outer leaflets can yield a spontaneous membrane curvature. These compositions are controlled by metabolic reactions on Golgi apparatus and lipid droplets^{9,10}, and by vesicular transport in cells. However, the evolution dynamics of lipid droplets on endoplasmic reticulum and the control of their sizes and shapes are not understood so far.

Recently, the shape evolution of vesicles and micelles induced by chemical reactions has been experimentally observed^{11–13}. In experiments conducted by Toyota *et al.*¹², amphiphilic molecules were divided into hydrophobic and hydrophilic molecules by hydrolysis. It was found that the resultant hydrophobic molecules induce a decrease in the spontaneous curvature of amphiphilic molecular assemblies, leading to various shape changes. Initially, these amphiphilic

molecules aggregate into a spherical micelle structure. As the chemical reaction progresses, this subsequently transforms into a tubular micelle, spherical vesicle, tubular vesicle, stomatocyte, and nested vesicle. Finally, the amphiphilic molecules form oil droplets. Through this reaction, a nanometer order structure (micelles) surprisingly changes to micrometer order structure (vesicles and droplets). This chemical reaction progresses slowly compared to vesicle shape deformation.

In experiments conducted by Takakura *et al.*¹³, hydrophobic and hydrophilic molecules are bound into amphiphilic molecules by dehydro-condensation. Initially, hydrophobic molecules are formed in an oil droplet in water. The chemical reaction occurs on the droplet surface and decreases the surface tension. Consequently, various complex structures (*e.g.*, multiple vesicles connected together by narrow necks) are observed. Using this chemical reaction, Takakura produced a self-reproducing system, in which new vesicles (daughter vesicles) are produced from oil droplets in the vesicles (mother vesicles). Self-reproduction is one of the main functions of protocells^{14–16}, and understanding the detailed mechanism of shape transformation induced by chemical reactions is important to improving self-reproduction control.

Although various shape deformations induced by chemical reactions are observed *in vitro* and *in vivo*, their mechanisms are not understood so far. The aim of this study is to clarify the shape transformation of the binding reaction to form amphiphilic molecules using coarse-grained molecular simulations. The lengths and time scales of all-atom simulations are still limited and, in order to simulate large-scale dynamics, various coarse-grained molecules are developed^{17–19}. In comparison with thermal equilibrium states, non-equilibrium dynamics including chemical reactions have been explored to a much lesser extent. Here, we propose a simple binding re-

Institute for Solid State Physics, University of Tokyo, Kashiwa, Chiba 277-8581, Japan. E-mail: noguchi@issp.u-tokyo.ac.jp

action model between one hydrophilic and one hydrophobic particle to form an amphiphilic molecule. We show how this reaction modifies the membrane properties and induces morphological changes.

In Section 2, our simulation model is described while, in Section 3, the shape transformation induced by chemical reaction is explained. Section 4 presents the effects of hydrophobic particles embedded in the bilayer membrane and Section 5 contains the summary and discussion.

2 Simulation Model and Method

2.1 Dissipative Particle Dynamics

Dissipative Particle Dynamics (DPD) is a coarse-grained molecular simulation method to take into account hydrodynamic interactions^{20–22}. The DPD method is applied to complex fluids such as amphiphilic molecules^{17,23–32} and polymers^{22,33–35}. In this method, several atoms are coarse-grained into one DPD particle, so long-term simulation can be performed compared to atomic-scale molecular dynamics.

In the DPD method, time evolutions are described using Newton's equation of motion with a pairwise Langevin thermostat, such that

$$\begin{aligned} \frac{d\mathbf{r}_i}{dt} &= \mathbf{v}_i, \quad m \frac{d\mathbf{v}_i}{dt} = \mathbf{f}_i, \\ \mathbf{f}_i &= \sum_{j \neq i} (\mathbf{F}_{ij}^C + \mathbf{F}_{ij}^D + \mathbf{F}_{ij}^R). \end{aligned} \quad (1)$$

The conservative force, \mathbf{F}_{ij}^C , is given by

$$\mathbf{F}_{ij}^C = a_{ij}(1 - r_{ij}/\sigma)\Theta(1 - r_{ij}/\sigma)\hat{\mathbf{r}}_{ij}, \quad (2)$$

where a_{ij} is the maximum repulsive force strength, σ is the cut-off length, $\mathbf{r}_{ij} = \mathbf{r}_i - \mathbf{r}_j$, and $\hat{\mathbf{r}}_{ij} = \mathbf{r}_{ij}/|\mathbf{r}_{ij}|$. The unit step function, $\Theta(x)$, is defined as

$$\Theta(x) = \begin{cases} 1 & (x > 0), \\ 0 & (\text{otherwise}). \end{cases} \quad (3)$$

The dissipation force, \mathbf{F}_{ij}^D , is given by

$$\mathbf{F}_{ij}^D = -\gamma_{ij}\omega^D(r_{ij})(\hat{\mathbf{r}}_{ij} \cdot \mathbf{v}_{ij})\Theta(1 - r_{ij}/\sigma)\hat{\mathbf{r}}_{ij}, \quad (4)$$

where $\mathbf{v}_{ij} = \mathbf{v}_i - \mathbf{v}_j$, γ_{ij} is a friction parameter and $\omega^D(r)$ is a weight function. The random force, \mathbf{F}_{ij}^R , is given by

$$\mathbf{F}_{ij}^R = \sigma_{ij}\omega^R(r_{ij})\zeta_{ij}(t)\Theta(1 - r_{ij}/\sigma)\hat{\mathbf{r}}_{ij}, \quad (5)$$

where σ_{ij} is noise strength and $\zeta_{ij}(t)$ is a Gaussian random number with the following properties:

$$\langle \zeta_{ij}(t) \rangle = 0, \quad (6)$$

$$\langle \zeta_{ij}(t)\zeta_{kl}(t') \rangle = 2(\delta_{ik}\delta_{jl} + \delta_{il}\delta_{jk})\delta(t - t'). \quad (7)$$

To satisfy the fluctuation dissipation theorem, γ_{ij} , σ_{ij} , $\omega^D(r)$, and $\omega^R(r)$ should be related via^{21,22}

$$\sigma_{ij}^2[\omega^R(r)]^2 = \gamma_{ij}k_B T \omega^D(r). \quad (8)$$

We choose $\omega^D(r) = [\omega^R(r)]^2 = (1 - r/\sigma)^2$.

In the DPD method, the random and dissipation forces act as pairwise forces. Since the action-reaction law is satisfied for each particle pair, the momentum conservation law is satisfied. Thus, the hydrodynamic interactions are taken into account.

2.2 Molecular Model

In this paper, W, H, and T denote a coarse-grained water, hydrophilic, and hydrophobic particle, respectively. For simplicity, the amphiphilic molecule is modeled by two soft particles connected by a spring force, such that

$$\mathbf{F}_{ij}^B = C(1 - r_{ij}/r_b)\hat{\mathbf{r}}_{ij}, \quad (9)$$

where C is the bond strength and r_b is the bond length. We set $C = 480k_B T/\sigma$ and $r_b = \sigma$. In order to form a bilayer membrane and an oil droplet, a_{ij} and γ_{ij} are set as shown in Table 1.

Table 1 Interaction parameters a_{ij} and γ_{ij} with units $k_B T/\sigma$ and $\sqrt{mk_B T}/\sigma$, respectively.

Bead pair	a_{ij}	γ_{ij}
WW	100	72
HH	100	72
TT	100	72
WH	100	72
WT	300	288
HT	200	144

The equations of motion are discretized by the modified Verlet algorithm²², such that

$$\mathbf{r}_i(t + \Delta t) = \mathbf{r}_i(t) + \mathbf{v}_i(t)\Delta t + \frac{\Delta t^2}{2m}\mathbf{f}_i(t), \quad (10)$$

$$\tilde{\mathbf{v}}_i(t + \Delta t) = \mathbf{v}_i(t) + \frac{\lambda\Delta t}{m}\mathbf{f}_i(t), \quad (11)$$

$$\mathbf{f}_i(t + \Delta t) = \mathbf{f}_i(\mathbf{r}_i(t + \Delta t), \tilde{\mathbf{v}}_i(t + \Delta t)), \quad (12)$$

$$\mathbf{v}_i(t + \Delta t) = \tilde{\mathbf{v}}_i(t + \Delta t) + \frac{\Delta t}{2m}(\mathbf{f}_i(t) + \mathbf{f}_i(t + \Delta t)). \quad (13)$$

Note that a large time step yields artifacts in DPD simulations³⁶. To avoid the emergence of such artifacts, the time step, Δt , is set to $0.005\sigma\sqrt{m/k_B T}$. The factor, λ , is often set to 0.65 in DPD simulations²². We compared the temperature difference between $\lambda = 0.5$ and $\lambda = 0.65$, but no apparent difference was detected between these values for

$\Delta t = 0.005\sigma\sqrt{m/k_B T}$. In both settings, the deviations of the configurational and kinetic temperatures from the specified value are less than 0.5%. Thus, λ is set to 0.5 in this study. The DPD program is originally implemented using CUDA³⁷.

All simulations are performed in the NVT ensemble (constant particle number, N , volume, V , and temperature, T) with the periodic boundary condition. The total number of particles is $N = N_H + N_T + N_W$, while the number density ρ of all particles is fixed as $\rho = 3\sigma^{-3}$. We use reduced units with σ as the unit of length, $k_B T$ as the unit of energy, and τ as the unit of time, where $\tau = \sigma^2/D$ with the diffusion constant, $D = 0.082\sigma\sqrt{k_B T/m}$, of W particles. The viscosity, η , of the W particle fluids is obtained as $\eta\sigma^2/\sqrt{mk_B T} = 4.0 \pm 0.1$ from the stress calculation in simple shear flow³⁸. Thus, our simulation condition yields a high Schmidt number for the DPD particles: $Sc = \eta/mpD = 16$. Since the momentum propagates significantly more rapidly than the mass, hydrodynamic interactions are taken into account in the diffusion of the DPD particles. As the typical lengths of lipids and other amphiphilic molecules is 1–3 nm, we can consider to be $\sigma \sim 1$ nm. Thus, the simulation time unit is estimated as $\tau \sim 0.6$ ns in water ($\eta = 0.8$ mPa·s) at room temperature.

2.3 Membrane Properties in the Absence of Hydrophobic Molecules

2.3.1 Bending Rigidity. The amphiphilic molecules, consisting of one hydrophilic (H) and one hydrophobic (T) particle, self-assemble into a fluid bilayer membrane in water. We estimate the bending rigidity, κ , of the membrane from the thermal fluctuations of a flat membrane^{17,39,40}. Using Monge parameterization, the membrane shape is described by the membrane height, $h(x, y)$, above the xy plane. According to the equipartition theorem, the thermal fluctuations of the membrane and κ are related via the equation¹

$$\langle |h(\mathbf{q})|^2 \rangle = \frac{k_B T}{\gamma|\mathbf{q}|^2 + \kappa|\mathbf{q}|^4}, \quad (14)$$

where γ is the surface tension of the membrane. The Fourier mode, $h(\mathbf{q})$, of $h(x, y)$ is given by

$$h(\mathbf{q}) = \frac{1}{\sqrt{A}} \int h(x, y) \exp(-i\mathbf{q} \cdot \mathbf{r}) dx dy, \quad (15)$$

where A is the membrane area. We estimate κ from eqn (14) for a tensionless membrane ($\gamma = 0$). The size of the simulation box is set to $32\sigma \times 32\sigma \times 32\sigma$. For the tensionless membrane, the number of amphiphiles, N_{amp} , is 4700 and the area per amphiphile is $0.4357\sigma^2$. The bending rigidity is obtained as $\kappa = 18.0 \pm 0.3k_B T$.

2.3.2 Edge Line Tension. We estimate the line tension, Γ , of the membrane edge from a membrane strip. The line

tension is calculated from^{41,42}

$$\Gamma = \left\langle \frac{P_{xx} + P_{zz}}{2} - P_{yy} \right\rangle \frac{L_z L_x}{2}, \quad (16)$$

with

$$P_{\alpha\alpha} = \frac{1}{V} \left(Nk_B T + \sum_{i>j} (\alpha_i - \alpha_j) F_{ij\alpha}^C \right), \quad (17)$$

where $\alpha \in x, y, z$, $F_{ij\alpha}^C$ is the α component of \mathbf{F}_{ij}^C , and L_α is the simulation box length along the α axis. The strip is along the y axis and the edge line length is $2L_y$. We estimate Γ for several line lengths, L_y/σ , from 17 to 21, at $L_z = L_x = 32\sigma$ and $N_{\text{amp}} = 1000$, and take the average for different values of L_y . The line tension is obtained as $\Gamma = 6.1 \pm 0.2k_B T/\sigma$.

2.4 Chemical Reaction Model

In this paper, we consider only a binding chemical reaction between hydrophilic and hydrophobic molecules forming an amphiphilic molecule, so that the inverse reaction (bond dissociation) is neglected. The chemical reaction is phenomenologically introduced as a stochastic process for a neighbor pair of H and T particles. For the reacted pair, the spring force, eqn (9), is added between the H and T particles. In each simulation time step, the binding probability, $P(r_{ij})$, is calculated from the particle distance, with

$$P(r_{ij})\Delta t = \begin{cases} p_0 \Theta(1 - r_{ij}/\sigma) \exp\left[-\frac{r_{ij}^2}{2x_0^2}\right] & ((i, j) = (H, T) \\ & \text{or } (T, H)), \\ 0 & (\text{otherwise}), \end{cases} \quad (18)$$

where p_0 is the chemical reaction rate and x_0 is the chemical reaction length scale. We set $p_0 = 1$ and $\sigma^2/x_0^2 = 20$. Thus, $x_0 \simeq 0.223\sigma$.

3 Shape Deformation Induced by Chemical Reaction

As an initial condition, hydrophobic particles are centered in water, as shown in Fig. 1. The hydrophobic particles form a spherical droplet through hydrophobic interactions. This droplet structure is called an oil droplet in the following. The hydrophilic particles are dispersed in water and no amphiphilic molecules initially exist. The number of hydrophilic, hydrophobic and total particles are $N_H = 12403$, $N_T = 6566$, and $N = 145920$, respectively. After equilibrating the system for 4τ steps, the chemical reaction as described in Section 2.4 is activated.

A typical example of shape deformation dynamics is shown in Fig. 2. The binding reaction occurs on the surface of an oil droplet. Through this reaction, the surface tension of the oil

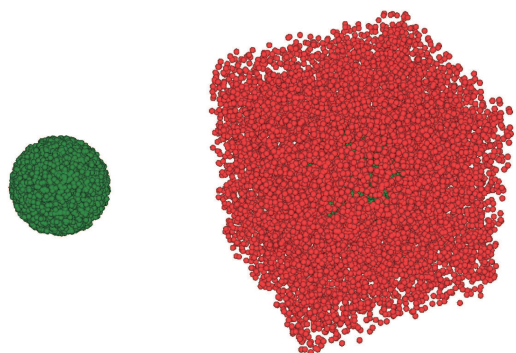


Fig. 1 Snapshot of initial state of an oil droplet at $N_H = 12403$, $N_T = 6566$, and $N = 145920$. The unreacted hydrophobic (green) particles are only shown in the left panel. Hydrophilic (red) particles are also shown in the right panel. Water particles are not shown for clarity.

droplet decreases so that the area increases. As the chemical reaction progresses, the oil droplet transforms to a disk micelle called bicelle (see Fig. 2(a)). Subsequently, the bicelle closes into a vesicle via a bowl-like shape (see Fig. 2(b)). This closing transition will be discussed later, in Section 4. In this spherical vesicle, unreacted hydrophobic particles are still embedded in the bilayer membrane. As the chemical reaction proceeds, a discoidal arm grows from the vesicle (see Fig. 2(c)), which then closes to form an additional vesicle (see Fig. 2(d)). The two vesicles are connected to a stalk-like structure, which is observed during the membrane fusion^{43–45}. The unreacted hydrophobic particles are concentrated on the stalk region, and the two vesicles are fused into a single large tubular vesicle (see Fig. 2(f)). During this fusion process, the region connecting two vesicles expands into a flat membrane, as shown in Fig. 2(e). This fusion pathway is similar to the stalk-bending (or stalk-leaky) pathway reported in Ref.^{43–45}. In the present system, the stalk expansion is provoked by the chemical reaction.

To quantify the shape deformation induced by the chemical reaction, we calculate three quantities: the radius of gyration, R_g , the surface area, A_{amp} , of the amphiphilic molecular assembly, and the ratio of chemically reacted particles, $n_{chem} = N_{amp}/N_T$, as shown in Fig. 3. The radius of gyration is defined as $R_g^2 = \sum_i |r_i - r_G|^2 / N_{ass}$, where r_G and N_{ass} are the center of mass and number of particles in the amphiphilic molecular assembly, respectively. At $t/\tau \lesssim 1000$, R_g increases and decreases repeatedly, as shown in Fig. 3(a). These increases and decreases indicate discoidal arm growth and vesicle closure, respectively.

A_{amp} is calculated as follows. First, the simulation box is divided into small cubic boxes with side length σ , and then the number, n_{amp} , of hydrophobic and reacted hydrophilic par-

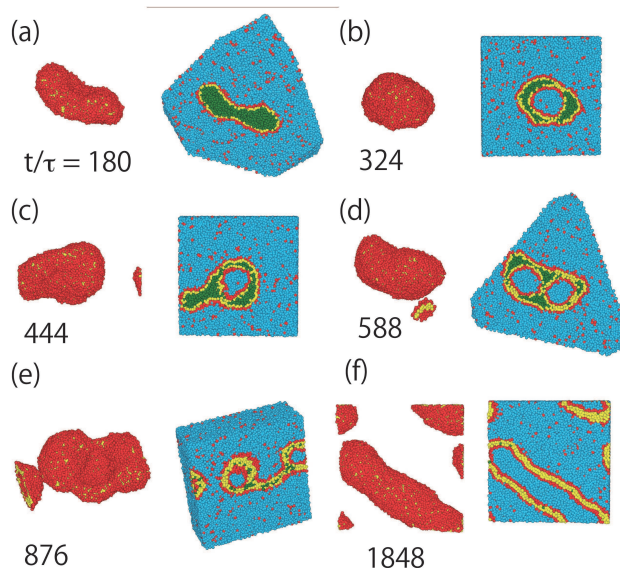


Fig. 2 Sequential snapshots of an amphiphilic molecular assembly under the binding reaction at $N_H = 12403$, $N_T = 6566$, and $N = 145920$. The number represent the simulation time t/τ . The yellow particles represent the reacted hydrophobic particles. Sliced snapshots with water (blue) particles are shown on the right side.

ticles in each box is counted. Second, the boxes in which $n_{amp} \geq n_{cut}$ are extracted. Here, the cut-off number, n_{cut} , is set to 2. Third, the number, N_{wface} , of the small box faces that are exposed to water is counted ($n_{amp} < n_{cut}$). The surface area is estimated from $A_{amp} = N_{wface} \sigma^2$.

A_{amp} monotonically increases, as shown in Fig. 3(b). Since the amphiphilic particles prefer to be on the surface of the amphiphilic assembly, the increase in A_{amp} is linear to an increase in the reaction ratio, n_{chem} . This fact is clear from comparison between Fig. 3 (b) and Fig. 3 (c).

To further clarify the chemical reaction progression, we compare the surface areas, A_{oil} , of the unreacted hydrophobic particles and the binding reaction rate, dn_{chem}/dt (see Fig. 4). A_{oil} is determined using the same procedure as for A_{amp} . As shown in Figs. 4 (a) and (b), there is a positive correlation between the two quantities. Under the fluctuation of the amphiphilic assembly, the chemical reaction occurs on the surface of the oil droplet. Thus, dn_{chem}/dt is roughly proportional to A_{oil} .

For a larger oil droplet, more vesicles and arms are produced as intermediate states under the chemical reaction. We investigate the shape development at four parameter sets, as summarized in Table 2. Four independent runs are performed for each condition. In cases of $N_H = 13132$, $N_T = 10943$, and $N = 145920$ (bottom row in Table 2), three vesicles are produced from one oil droplet. In this case, an alternative final shape, that is, a toroidal shape, can be formed as, shown in

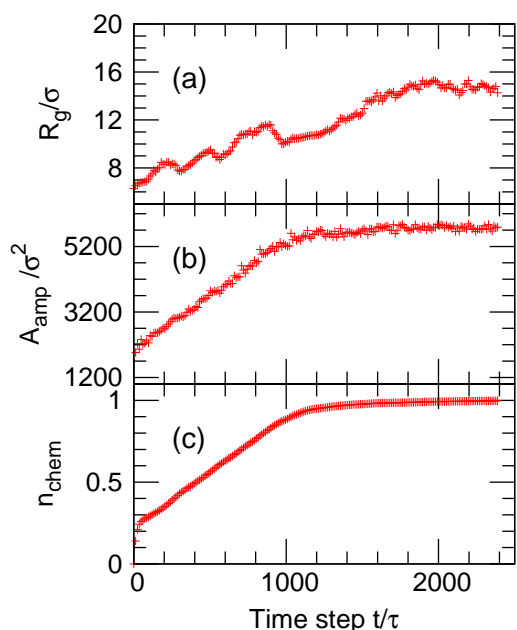


Fig. 3 Time development of (a) the radius of gyration, R_g , (b) area, A_{amp} , of the amphiphilic molecular assembly, and (c) chemical reaction ratio, $n_{chem} = N_{amp}/N_T$. The same data as in Fig. 2 is shown.

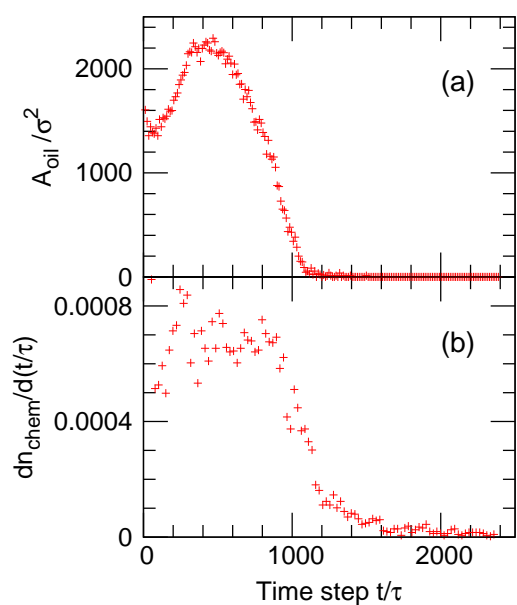


Fig. 4 Time development of (a) the area A_{oil} of unreacted hydrophobic particles and (b) the chemical reaction rate dn_{chem}/dt . The same data in Fig. 2 is shown.

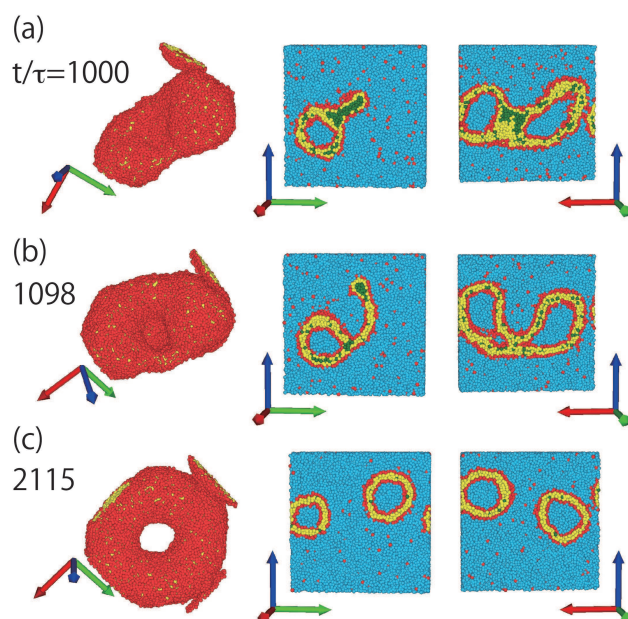


Fig. 5 Sequential snapshots of a shape transformation from an oil droplet into a toroidal vesicle at $N_H = 13132$, $N_T = 10943$, and $N = 145920$. Sliced views are shown in the middle and right rows and two sliced sections are perpendicular to each other. The red, green, and blue arrows indicate the x , y , and z directions, respectively.

Fig. 5. Whether the final shape is a tubular or toroidal vesicle depends on the existence of a certain intermediate shape, as shown in Fig. 5 (a). This intermediate shape is composed of a tubular vesicle and a flat membrane, which is attached to the side of the tubular vesicle. The tubular vesicle is bent around the disk. Then, the ends of the tubular vesicle are fused together, resulting in the formation of the toroidal vesicle (see Figs. 5 (b) and (c)). This bending process is similar to the bending of the stalk shown in Fig. 2(e). Thus, the bending around the neighboring compartment is a type of generic dynamics for amphiphilic systems.

Table 2 Final shapes generated from oil droplets for four simulation settings. Four independent runs are executed for each setting. The fourth/fifth row indicate the number of simulation samples with tubular or toroidal vesicle shapes.

N_H	N_T	N	Tubular	Toroidal
12403	6566	145920	4	0
11424	8601	134400	3	1
13132	10214	145920	4	0
13132	10943	145920	3	1

4 Effects of Embedded Hydrophobic Particles

In the simulations described in Section 3, we notice that the shape transition from bicelle to vesicle is enhanced by the chemical reaction. The vesicle is formed from smaller membranes in comparison to those only consisting of amphiphilic molecules. Since the transition occurs under non-equilibrium conditions, this enhancement may be caused by some dynamic effects due to inhomogeneity of the reaction and hydrodynamic interactions, or by changes in the membrane properties due to embedded hydrophobic particles. To clarify whether the enhancement is caused by dynamic or static effects, we simulate the bicelle-to-vesicle transition of the membrane with embedded hydrophobic particles in the absence of the chemical reaction (Section 4.1). It is revealed that the transition is enhanced by the embedded particles. Next, we investigate the dependence of the transition on the membrane properties (Section 4.2 and 4.3) and conclude that the enhancement is caused by the reduction of the bending rigidity (Section 4.4).

4.1 Enhancement of Bicelle-to-Vesicle Transition

We use the method proposed by Hu et al.⁴⁶ to calculate the free energy barrier between bicelle and vesicle. This method was originally used for determining the Gaussian curvature modulus, $\bar{\kappa}$. Here, we briefly summarize this method.

For a homogeneous membrane, the shape transition from bicelle to vesicle is understood by the competition between the edge-line and bending energies of the membrane⁴⁷. The bicelle has edge energy of $2\pi R_{\text{dis}}\Gamma$ and no bending energy, where $R_{\text{dis}} = \sqrt{A/\pi}$ is the radius of the bicelle of the membrane area, A . The vesicle has bending energy of $8\pi(\kappa + \bar{\kappa}/2)$ and no edge energy. An intermediate shape during the shape transition can be approximated as a spherical cap around the transition point⁴⁸. Under this geometrical assumption, the excess energy, ΔE , of the membrane with respect to the flat bicelle is given by^{46,47}

$$\Delta E(\Omega^2, \zeta) = 4\pi(2\kappa + \bar{\kappa})[\Omega^2 + \zeta(\sqrt{1 - \Omega^2} - 1)], \quad (19)$$

$$\zeta = \frac{\Gamma R_{\text{ves}}}{2\kappa + \bar{\kappa}}, \quad \Omega = \frac{R_{\text{ves}}}{R}, \quad \text{and } R_{\text{ves}} = \sqrt{\frac{A}{4\pi}}, \quad (20)$$

where $1/R$ is the curvature of the membrane. The normalized curvature, Ω , is an order parameter: $\Omega = 0$ and 1 for the bicelle and vesicle, respectively. At $\zeta = 1$, the bicelle and vesicle have the same energy and, for $0 < \zeta < 2$, a free energy barrier exists at $0 < \Omega < 1$.

The free energy barrier can be determined by collecting samples in which pre-curved membranes change into open disks or closed vesicles. The probability, $P(\Omega^2)$, at which the pre-curved membranes change into closed vesicles, is derived

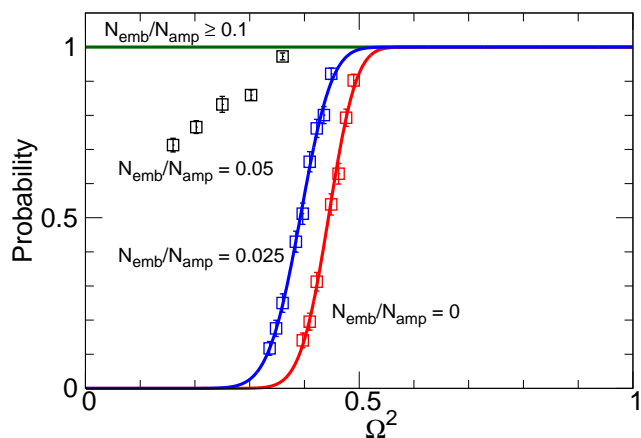


Fig. 6 Transition probability to a vesicle as a function of Ω^2 . The squares represent the simulation data for $N_{\text{emb}}/N_{\text{amp}} = 0, 0.025$, and 0.05 . The red and blue solid lines represent fits by eqn (21) for $N_{\text{emb}}/N_{\text{amp}} = 0$ and 0.025 , respectively. At $N_{\text{emb}}/N_{\text{amp}} \geq 0.1$, the transition probability becomes unity, independent of Ω^2 (green solid line).

for the initial Ω as⁴⁶

$$P(\Omega^2) = \frac{\int_0^{\Omega^2} dy \exp(\Delta E(y, \zeta)/\tilde{D})}{\int_0^1 dy \exp(\Delta E(y, \zeta)/\tilde{D})}. \quad (21)$$

By fitting this function to simulation data, \tilde{D} and ζ are determined. The free energy barrier of eqn (19) is obtained from the value of ζ . We execute 512 independent runs for each parameter set (Ω, N_{emb}) , and calculate the free energy barrier between the bicelle and vesicle. In the simulation, $N = 41472$, $N_{\text{amp}} = 1000$, and $N_{\text{emb}} = 25, 50, 100, 300$, and 500 are used.

The $P(\Omega^2)$ curves at $N_{\text{emb}}/N_{\text{amp}} = 0$ and 0.025 are well fit by eqn (21) with $(\zeta, \tilde{D}) = (1.49, 0.00147)$ and $(1.56, 0.00174)$, respectively (see Fig. 6). As the hydrophobic particles are increasingly embedded, $P(\Omega^2)$ increases. Thus, the free energy barrier is decreased by the embedded hydrophobic particles. Surprisingly, no barrier exists for $N_{\text{emb}}/N_{\text{amp}} \geq 0.1$. To clarify the causes of this decrease in the free energy barrier, we investigate the dependence of the membrane properties on $N_{\text{emb}}/N_{\text{amp}}$ in the next two subsections.

4.2 Bending Rigidity

We estimate the bending rigidity, κ , of the membrane containing hydrophobic particles. Since the area of the tensionless membrane depends on the fraction of embedded hydrophobic particles, we set the tensionless state by changing N_{amp} for a fixed value of N_{emb} . For each zero-surface-tension state, the method described in Section 2.3.1 is applied to calculate κ .

As the embedded hydrophobic particles are added, κ first decreases and is saturated at $N_{\text{emb}}/N_{\text{amp}} \gtrsim 0.15$ (see Fig. 7).

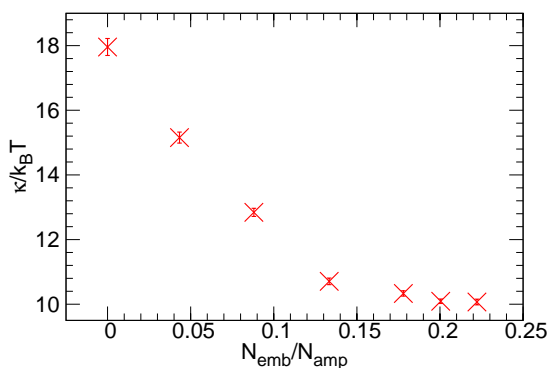


Fig. 7 Bending rigidity, κ , dependence on $N_{\text{emb}}/N_{\text{amp}}$.

To explain this dependence, we calculate two quantities of the bilayer membrane that may cause the change in the bending rigidity. One is the bilayer thickness, d , and the other is the orientational order parameter, S . The orientational order is expressed by

$$S = \left\langle \frac{3n_{i,z}^2 - 1}{2} \right\rangle, \quad (22)$$

where $n_{i,z}$ is the z component of the unit vector of the i -th amphiphilic molecule from the hydrophobic to hydrophilic particles.

For the homogeneous membrane in the absence of hydrophobic molecules, κ has the following relationships with the orientational order and thickness. The orientational order of the amphiphiles is related to the membrane bending fluctuations according to^{49,50}

$$\langle |n_q^{\parallel}|^2 \rangle = \frac{k_B T}{\kappa q^2}, \quad (23)$$

where $n_q^{\parallel} = [\mathbf{q} \cdot \mathbf{n}_q]/q$, n_q is the Fourier transformation of the amphiphilic orientational vector, \mathbf{n} . On the other hand, the membrane thickness, d , is related to κ via the equation⁵¹

$$\kappa = \frac{1}{48} Y d^3, \quad (24)$$

where Y is the Young modulus. However, the heterogeneous membrane with embedded particles may not obey these relations.

The dependence of d and S of the embedded membranes on $N_{\text{emb}}/N_{\text{amp}}$ are shown in Fig. 8. Following addition of the hydrophobic particles, d increases and S decreases. The embedded hydrophobic particles disturb the orientation of the amphiphiles, and enlarge d . The decrease in S is saturated at $N_{\text{emb}}/N_{\text{amp}} \gtrsim 0.15$ but d shows no saturation.

According to eqn (24), κ increases with increasing d . However, adding more hydrophobic particles decreases κ despite the increasing d . This is likely due to the rearrangement of

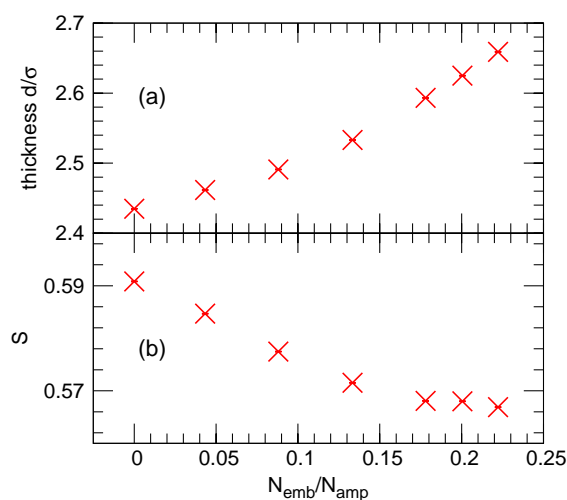


Fig. 8 Dependence of (a) the orientational order parameter, S and (b) the membrane thickness, d , on $N_{\text{emb}}/N_{\text{amp}}$.

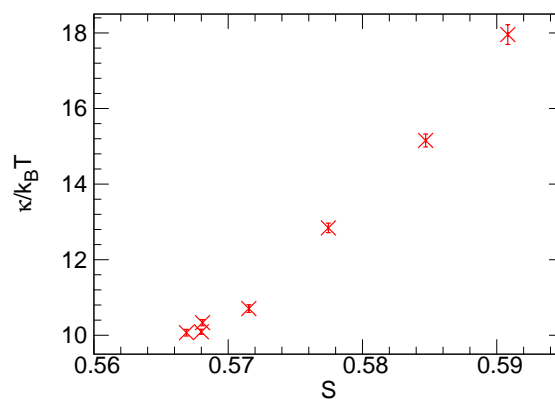


Fig. 9 Bending rigidity, κ , as a function of the orientational order, S .

the positions of the hydrophobic particles in the bilayer. In a curved membrane, the embedded hydrophobic particles can exist more in the outer (laterally expanded) leaflet than in the inner leaflet. In contrast, the change in S is similar to the change in κ . In order to illustrate this more clearly, we replot κ as a function of S in Fig. 9. The linear relation between κ and S is clear. Thus, the reduction of κ by the embedded particles is mainly caused by the disturbance of the orientation of the amphiphilic molecules.

4.3 Edge Line Tension

We estimate the edge line tension, Γ , at $N_{\text{emb}}/N_{\text{amp}} = 0$ to 0.5 (see Fig. 10). At $N_{\text{emb}}/N_{\text{amp}} \lesssim 0.1$, Γ is almost constant. For $N_{\text{emb}}/N_{\text{amp}} \in [0.1, 0.3]$, Γ increases, while for $N_{\text{emb}}/N_{\text{amp}} > 0.3$, Γ decreases. At $N_{\text{emb}}/N_{\text{amp}} > 0.3$, the hydrophobic par-

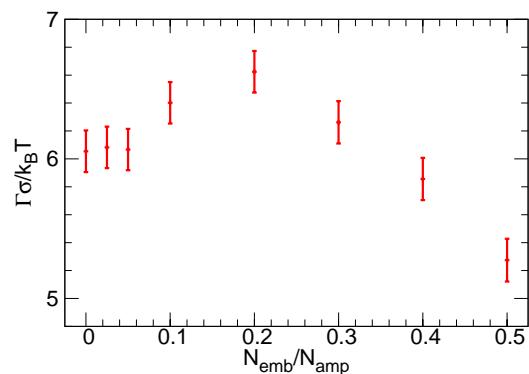


Fig. 10 Edge line tension, Γ , as a function of $N_{\text{emb}}/N_{\text{amp}}$.

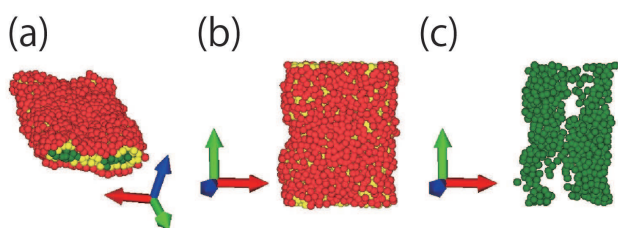


Fig. 11 Snapshots of the membrane strip at $N_{\text{emb}}/N_{\text{amp}} = 0.5$ and $L_y = 17\sigma$. Embedded hydrophobic particles are only shown in (c) from the same view point as in (b).

ticles are concentrated at the membrane edge and the membrane forms swollen round edges (see Fig. 11). This reduction of the edge curvature would cause a reduction in Γ . For $N_{\text{emb}}/N_{\text{amp}} \in [0.1, 0.3]$, the density of the hydrophobic particles is not uniform on the membrane edge. Thus, the membrane tends towards a shorter edge at which the hydrophobic particles can be uniformly distributed. This tendency likely enhances Γ .

4.4 Origin of Enhancement Effect

By using the results shown in the previous two subsections, the enhancement effect of the bicelle-to-vesicle transition is understood by the change in the membrane properties. According to the results of Section 4.3, the change in Γ is apparent only for $N_{\text{emb}}/N_{\text{amp}} \geq 0.1$. However, the enhancement effect is apparent even for $N_{\text{emb}}/N_{\text{amp}} \simeq 0.025$, as shown in Fig. 6. Thus, the line tension is not a relevant parameter for the enhancement. In contrast, the change in κ is apparent for $N_{\text{emb}}/N_{\text{amp}} \lesssim 0.15$.

The ratio, $\bar{\kappa}/\kappa = -1.06$, is obtained from the simulations at $N_{\text{emb}} = 0$. This is a typical value for lipid membranes ($\bar{\kappa}/\kappa \simeq -1$)⁴⁶. We assume that $\bar{\kappa}/\kappa$ is independent of $N_{\text{emb}}/N_{\text{amp}}$. At $N_{\text{emb}}/N_{\text{amp}} \simeq 0.1$, the parameter, $\zeta \simeq 2.2$, is obtained from $\kappa/k_B T \simeq 12.4$. This agrees with the results of the transition

simulation, i.e., that all membranes transform into vesicles, since the free energy barrier disappears at $\zeta \geq 2$.

In order to more quantitatively verify this, we compare two ratios c_κ and c_ζ , which are defined as

$$c_\kappa = \frac{\kappa(0)}{\kappa(0.025)} \quad \text{and} \quad c_\zeta = \frac{\zeta(0.025)}{\zeta(0)}, \quad (25)$$

where $\kappa(0)$ and $\zeta(0)$ ($\kappa(0.025)$ and $\zeta(0.025)$) denote κ and ζ at $N_{\text{emb}}/N_{\text{amp}} = 0$ (0.025), respectively. When $\bar{\kappa}/\kappa$ and Γ are constant, $c_\kappa = c_\zeta$. In the region of $N_{\text{emb}}/N_{\text{amp}} \in [0, 0.1]$, $\kappa(N_{\text{emb}}/N_{\text{amp}})$ can be well fitted by the linear function, $\kappa(x)/k_B T = ax + b$, for $(a, b) = (52 \pm 3, 17.5 \pm 0.3)$. We calculate $\kappa(0.025)$ using this fit function. It gives $c_\kappa = 1.07 \pm 0.03$ and $c_\zeta = 1.045 \pm 0.002$, so that they coincide within the statistical error. Thus, we conclude that the enhancement of the transition is caused by the reduction of κ .

The inclusion of molecules such as sterols and peptides modifies the bending rigidity, which also depends on lipid composition and buffer conditions^{52–55}. The addition of cholesterol was previously believed to increase κ in general^{28,52}. Recently, however, Dimova et al. reported that κ is reduced for a sphingomyelin membrane and does not significantly change for DOPC membranes with increasing cholesterol content^{52,53}. The reduction of κ was also reported for the addition of the peptide, FP23,⁵² and azithromycin⁵⁴ to DOPC membranes. The inclusion of lidocaine increases κ , whereas d decreases in the L_α phase of DMPC/DMPG membranes⁵⁵. Thus, depending on the embedded molecules, the bicelle-to-vesicle transition can be enhanced or suppressed. In the present system, enhancement is obtained but the opposite effect (suppression) can be induced by a different type of inclusion. However, the effect can be predicted by measuring κ and Γ as functions of the inclusion density.

5 Summary

We have investigated shape evolutions of amphiphilic molecular assemblies induced by the binding reaction between hydrophilic and hydrophobic molecules using DPD simulations. Various shape transformations such as bicelle-to-vesicle transition, multiple vesicle formation, vesicle fusion, and toroidal vesicle formation are exhibited under the non-equilibrium condition. When all hydrophobic particles are reacted, the thermal equilibrium state is a spherical vesicle. However, the final shapes are tubular and toroidal vesicles stabilized by the volume and topological constraints, which are generated in shape evolution. During the shape changes, the hydrophobic particles embedded in the membrane modify the membrane properties and affect the dynamics. We have quantified this enhancement effects by calculating the line tension and bending rigidity. In particular, the reduction of the bending rigidity accelerates the bicelle-to-vesicle transition.

The extension of discoidal arms from the vesicles and the closure of additional vesicles are found in our simulations. The formation of multiple vesicles from an oil droplet has been experimentally observed by Takakura et al.¹³. We expect that similar arm-extension and closure processes occurred in their experiment.

In this paper, we consider only a simple binding reaction. The shape dynamics can be changed by reaction schemes and molecular compositions. The effects of inverse and other reactions on the shape evolutions and its dependence on molecular architecture are important topics for further investigations.

Acknowledgments

We would like to thank T. Sugawara and T. Toyota for informative discussions. This work was supported by Japan Society for the Promotion of Science through Program for Leading Graduate Schools (MERIT) and a Grant-in-Aid for Scientific Research on Innovative Areas 'Fluctuation & Structure' (No. 25103010) from the Ministry of Education, Culture, Sports, Science, and Technology of Japan. The numerical calculations were partly carried out on SGI Altix ICE 8400EX and FUJITSU PRIMEHPC FX10 at ISSP Supercomputer Center, University of Tokyo.

References

- 1 S. A. Safran, *Statistical thermodynamics of surfaces, interfaces, and membranes*, Addison-Wesley Reading, MA, 1994.
- 2 I. W. Hamley, *Introduction to soft matter: synthetic and biological self-assembling materials*, John Wiley & Sons, 2008.
- 3 A. Walther and A. H. Müller, *Chem. Rev.*, 2013, **113**, 5194–5261.
- 4 *Structure and Dynamics of Membranes*, ed. R. Lipowsky and E. Sackmann, Elsevier Science, Amsterdam, 1995.
- 5 U. Seifert, *Adv. Phys.*, 1997, **46**, 13–137.
- 6 S. Svetina, *ChemPhysChem*, 2009, **10**, 2769–2776.
- 7 M. Yanagisawa, M. Imai and T. Taniguchi, *Phys. Rev. Lett.*, 2008, **100**, 148102.
- 8 A. Sakashita, M. Imai and H. Noguchi, *Phys. Rev. E*, 2014, **89**, 040701(R).
- 9 T. Fujimoto and R. G. Parton, *Cold Spring Harb. Perspect. Biol.*, 2011, **3**, a004838.
- 10 A. Pol, S. P. Gross and R. G. Parton, *J. Cell Biol.*, 2014, **204**, 635–646.
- 11 K. Suzuki, T. Toyota, K. Takakura and T. Sugawara, *Chem. Lett.*, 2009, **38**, 1010–1015.
- 12 T. Toyota, K. Takakura, J. Kose and T. Sugawara, *ChemPhysChem*, 2006, **7**, 1425–7.
- 13 K. Takakura, T. Toyota and T. Sugawara, *J. Am. Chem. Soc.*, 2003, **125**, 8134–40.
- 14 H. H. Zepik and P. Walde, *ChemBioChem*, 2008, **9**, 2771–2772.
- 15 P. Stano and P. L. Luisi, *Chem. Commun.*, 2010, **46**, 3639–3653.
- 16 K. Kurihara, M. Tamura, K.-i. Shohda, T. Toyota, K. Suzuki and T. Sugawara, *Nature Chem.*, 2011, **3**, 775–781.
- 17 M. Venturoli, M. Maddalenasperotto, M. Kranenburg and B. Smit, *Phys. Rep.*, 2006, **437**, 1–54.
- 18 S. J. Marrink, A. H. de Vries and D. P. Tieleman, *Biochim. Biophys. Acta*, 2009, **1788**, 149–168.
- 19 H. Noguchi, *J. Phys. Soc. Jpn.*, 2009, **78**, 041007.
- 20 P. J. Hoogerbrugge and J. M. V. A. Koelman, *Europhys. Lett.*, 1992, **19**, 155–160.
- 21 P. Espanol and P. Warren, *Europhys. Lett.*, 1995, **30**, 191.
- 22 R. D. Groot and P. Warren, *J. Chem. Phys.*, 1997, **107**, 4423.
- 23 M. Venturoli and B. Smit, *PhysChemComm*, 1999, **2**, 45–49.
- 24 R. D. Groot and K. L. Rabone, *Biophys. J.*, 2001, **81**, 725–736.
- 25 S. Yamamoto, Y. Maruyama and S.-a. Hyodo, *J. Chem. Phys.*, 2002, **116**, 5842–5849.
- 26 L. Gao, R. Lipowsky and J. Shillcock, *Soft Matter*, 2008, **4**, 1208–1214.
- 27 S. Ramachandran, M. Laradji and P. B. Sunil Kumar, *J. Phys. Soc. Jpn.*, 2009, **78**, 041006.
- 28 F. J.-M. de Meyer, A. Benjamini, J. M. Rodgers, Y. Misteli and B. Smit, *J. Phys. Chem. B*, 2010, **114**, 10451–1461.
- 29 F. M. Thakkar and K. G. Ayappa, *J. Chem. Phys.*, 2011, **135**, 104901.
- 30 N. Arai, K. Yasuoka and X. Zeng, *Microfluid. Nanofluid.*, 2013, **14**, 995–1010.
- 31 H.-L. Wu, P.-Y. Chen, C.-L. Chi, H.-K. Tsao and Y.-J. Sheng, *Soft Matter*, 2013, **9**, 1908–1919.
- 32 D. A. Fedosov, H. Noguchi and G. Gompper, *Biomech. Model. Mechanobiol.*, 2014, **13**, 239–258.
- 33 W. Tschöp, K. Kremer, J. Batoulis, T. Bürger and O. Hahn, *Acta Polymerica*, 1998, **49**, 61–74.
- 34 P. Nikunen, I. Vattulainen and M. Karttunen, *Phys. Rev. E*, 2007, **75**, 036713.
- 35 X. Li, M. Deng, Y. Liu and H. Liang, *J. Phys. Chem. B*, 2008, **112**, 14762–5.
- 36 M. P. Allen, B. D. Butler, G. Ayton, O. G. Jepps and D. J. Evans, *J. Phys. Chem. B*, 2006, **110**, 3823–30.
- 37 H. Nguyen, *Gpu gems 3*, Addison-Wesley Professional, 2007.
- 38 H. Noguchi and G. Gompper, *EPL*, 2007, **78**, 36002.
- 39 R. Goetz, G. Gompper and R. Lipowsky, *Phys. Rev. Lett.*, 1999, **82**, 221–224.
- 40 H. Shiba and H. Noguchi, *Phys. Rev. E*, 2011, **84**, 031926.
- 41 T. V. Tolpekina, W. K. den Otter and W. J. Briels, *J. Chem. Phys.*, 2004, **121**, 8014–20.
- 42 H. Noguchi, *J. Chem. Phys.*, 2011, **134**, 055101.
- 43 H. Noguchi and M. Takasu, *J. Chem. Phys.*, 2001, **115**, 9547.
- 44 M. Müller and M. Schick, *Curr. Top. Membr.*, 2011, **68**, 295–323.
- 45 H. J. Risselada, G. Bubnis and H. Grubmüller, *Proc. Natl. Acad. Sci. USA*, 2014, **111**, 11043–11048.
- 46 M. Hu, J. J. Briguglio and M. Deserno, *Biophys. J.*, 2012, **102**, 1403–10.
- 47 P. Fromherz, *Chem. Phys. Lett.*, 1983, **94**, 259–266.
- 48 H. Noguchi and G. Gompper, *J. Chem. Phys.*, 2006, **125**, 164908.
- 49 M. C. Watson, E. S. Penev, P. M. Welch and F. L. H. Brown, *J. Chem. Phys.*, 2011, **135**, 244701.
- 50 M. C. Watson, E. G. Brandt, P. M. Welch and F. L. H. Brown, *Phys. Rev. Lett.*, 2012, **109**, 028102.
- 51 L. D. Landau, E. M. Lifchits, A. M. Kosevitch, L. P. Pitaevski, J. B. Sykes, W. Reid, L. D. Landau and L. P. Pitaevski, *Course of theoretical physics: theory of elasticity*, Butterworth-Heinemann, 1986.
- 52 R. Dimova, *Adv. Colloid Interface Sci.*, 2014, **208**, 225–234.
- 53 R. S. Gracià, N. Bezlyepkina, R. L. Knorr, R. Lipowsky and R. Dimova, *Soft Matter*, 2010, **6**, 1472.
- 54 N. Fa, L. Lins, P. J. Courttoy, Y. Dufrêne, P. Van Der Smissen, R. Brasseur, D. Tyteca and M.-P. Mingeot-Leclercq, *Biochim. Biophys. Acta*, 2007, **1768**, 1830–1838.
- 55 Z. Yi, M. Nagao and D. P. Bossev, *Biophys. Chem.*, 2012, **160**, 20–27.